

Extremely Slow Diffusion of Gold Nanoparticles under Confinement in Mesoporous Silica

R. Mhanna, A. Fluerasu

To be published in "JOURNAL OF PHYSICAL CHEMISTRY C"

February 2022

Photon Sciences

Brookhaven National Laboratory

U.S. Department of Energy

USDOE Office of Science (SC), Basic Energy Sciences (BES) (SC-22)

Notice: This manuscript has been authored by employees of Brookhaven Science Associates, LLC under Contract No. DE-SC0012704 with the U.S. Department of Energy. The publisher by accepting the manuscript for publication acknowledges that the United States Government retains a non-exclusive, paid-up, irrevocable, world-wide license to publish or reproduce the published form of this manuscript, or allow others to do so, for United States Government purposes.

DISCLAIMER

This report was prepared as an account of work sponsored by an agency of the United States Government. Neither the United States Government nor any agency thereof, nor any of their employees, nor any of their contractors, subcontractors, or their employees, makes any warranty, express or implied, or assumes any legal liability or responsibility for the accuracy, completeness, or any third party's use or the results of such use of any information, apparatus, product, or process disclosed, or represents that its use would not infringe privately owned rights. Reference herein to any specific commercial product, process, or service by trade name, trademark, manufacturer, or otherwise, does not necessarily constitute or imply its endorsement, recommendation, or favoring by the United States Government or any agency thereof or its contractors or subcontractors. The views and opinions of authors expressed herein do not necessarily state or reflect those of the United States Government or any agency thereof.

Extremely Slow Diffusion of Gold Nanoparticles under Confinement in Mesoporous Silica

Ramona Mhanna,^{†,#} Michael Giroux,[‡] Kenneth J. T. Livi,[¶] Chao Wang,[‡] Andrei Fluerasu,[§] Lutz Wiegart,[§] Yugang Zhang,^{||} Mark Sutton,[⊥] and Robert L. Leheny^{*,†}

[†]*Department of Physics and Astronomy, Johns Hopkins University, Baltimore, Maryland
21218, USA.*

[‡]*Department of Chemical and Biomolecular Engineering, Johns Hopkins University,
Baltimore, Maryland 21218, USA.*

[¶]*Department of Materials Science and Engineering, Johns Hopkins University, Baltimore,
Maryland 21218, USA.*

[§]*National Synchrotron Light Source II, Brookhaven National Laboratory, Upton, NY 11973
USA.*

^{||}*Center for Functional Nanomaterials, Brookhaven National Laboratory, Upton, NY
11973, USA.*

[⊥]*Department of Physics, McGill University, Montréal, Québec H3A 2K6, Canada*

[#]*Current address: Colorado School of Mines, Golden, CO 80401, USA.*

E-mail: leheny@jhu.edu

Abstract

We report an x-ray photon correlation spectroscopy (XPCS) study of the mobility of colloidal gold nanoparticles with diameter approximately 4 nm in glycerol under

confinement within the channels of SBA-15 mesoporous silica with pore diameters of approximately 6 nm and 12 nm. The XPCS correlation functions result from an effective heterodyne signal due to the mixing of the coherent scattering from the nanoparticles and the mesoporous silica. Over the range of wave vectors and hence length scales probed, the nanoparticle dynamics are well described by one-dimensional diffusion. The nanoparticle diffusivity varies with temperature in a manner expected based on the temperature-dependent viscosity of glycerol; however, the magnitudes of the diffusion coefficients are several orders of magnitude smaller than those of the nanoparticles in bulk glycerol. We consider mechanisms that might contribute to this reduction in diffusivity including enhancement in hydrodynamic drag under confinement, effects of nanoparticle adsorption to the pore walls, and slowing structural dynamics in the glycerol due to the combination of the nanometer-scale confinement and the presence of the nanoparticles.

Introduction

The mobility of nanoscale particles suspended in fluids within confined geometries impacts a wide range of fields including biotechnology, catalysis, nanofabrication, lubrication, and environmental remediation.¹ Under nanometer-scale confinement, the Brownian diffusion that nanoparticles typically experience in a bulk fluid can be radically altered due to hydrodynamic, surface, and other interactions that become paramount when the particles are restricted to remain in close proximity to the bounding surfaces.²⁻⁴ A number of experimental approaches have been employed to characterize nanoparticle mobility under such conditions.⁵⁻¹⁰ In particular, recent advances in transmission electron microscopy (TEM) in liquid environments have enabled detailed single-particle-tracking experiments that have investigated nanoparticle motion in fluids under nanoscale confinement,¹¹⁻¹⁷ and in several cases these studies have revealed dynamics that are orders of magnitude slower than the corresponding Brownian motion in bulk.^{12,13,17} Such microscopy methods are well suited for

tracking nanoparticles that are confined along one direction, such as between closely spaced parallel substrates. However, other important confinement geometries for nanoparticle mobility, such as within bulk nanoporous and mesoporous materials, present a challenge for established techniques. To address this issue, we have performed an x-ray photon correlation spectroscopy (XPCS) study of the dynamics of dilute dispersions of colloidal gold nanoparticles under confinement in the nanochannels of mesoporous SBA-15 silica. The ability of XPCS to track the motion of nanoparticles over nanometer-scale distances makes it an ideal probe for such studies.

In XPCS, like in dynamic light scattering (DLS) with visible light, fluctuations in the coherent scattering intensity from a material provide information about the material's dynamics. However, due to the much shorter wavelength of x-rays, XPCS can probe motions over significantly smaller distances. This advantage provides XPCS with unique access to a region of dynamic phase space at small length scales and long time scales that makes it particularly well matched for interrogating nanoparticle mobility under nanometer-scale confinement.¹⁸⁻²¹ Another strength of XPCS stems from the relatively large penetration depth of x-rays, which enables the technique to access the interior of optically opaque materials, a property we have exploited in probing the nanoparticle mobility within the mesoporous silica matrices. Leveraging these advantages, a number of previous studies have employed XPCS to interrogate nanoparticle dynamics under confinement in different contexts including in polymer thin films, where the nanoparticles served as probes of the local viscosity,²²⁻²⁴ in cross-linked and entangled polymeric systems, where the nanoparticle mobility can display violations of the Stokes-Einstein relation that provide insight into the hierarchical structural dynamics of the materials,²⁵⁻²⁷ and at dense concentrations in porous environments, where the effects of the confinement on collective dynamics have been reported.²⁸ Here, we employ the technique to examine the mobility of gold nanoparticles with diameter of approximately 4 nm in glycerol confined within the straight, monodisperse pores of SBA-15 silica templates. Templates with two pore diameters, $D_p \approx 6$ nm and 12 nm, were included in the

study. The measurements characterize the diffusion of the nanoparticles along the pore axes and find diffusion coefficients that depend strongly on the pore size and that are several orders of magnitude smaller than those of the nanoparticles in bulk glycerol. Nevertheless, the diffusion coefficients appear to follow a temperature dependence expected based on the viscosity of glycerol. We discuss several possible mechanisms for this strong reduction in nanoparticle mobility and propose that slowing structural dynamics of the glycerol due to the nanoconfinement in the presence of the nanoparticles is a major contributor.

Methods

Sample Synthesis

Synthesis of Au Nanoparticles

To avoid the need to transfer nanoparticles from aqueous solution into glycerol, we synthesized the colloidal gold particles directly in glycerol through the reduction of gold(III) chloride trihydrate salt ($\text{HAuCl}_4 \cdot 3\text{H}_2\text{O}$) with tert-butylamine borane (BTB) in the presence of trioctylphosphine (TOP) as a capping agent. All chemicals were purchased from Sigma-Aldrich and used as received. In a typical procedure, 0.5 mmol (0.22 ml) TOP was injected into a solution of 0.5 g of $\text{HAuCl}_4 \cdot 3\text{H}_2\text{O}$ in 20 ml glycerol at 15 C after the reaction system had been sealed and purged with argon. 0.5 mmol BTB was solvated in 2 ml glycerol, sonicated for 10 minutes, and briefly heated with a heat gun to decrease the solvent viscosity before being injected into the gold solution. Directly after the injection of the reducing agent, a color change from yellow to light purple was observed. The resulting solution was then heated to 30 C for 1 hour under continuous argon flow. After the end of the reaction, the solution was cooled to room temperature, and the gold nanoparticles were extracted by adding 50 mL of isopropanol as a precipitant, followed by centrifugation (10000 rpm for 10 min). The TOP-stabilized gold nanoparticles were then re-dispersed in

glycerol via probe sonication. The final concentration of nanoparticles in the glycerol was approximately 0.25% by volume. The nanoparticles were characterized by transmission electron microscopy (TEM), which revealed a particle radius of about 1.45 nm with a standard deviation of 0.29 nm. Figure S1 of the Supporting Information (SI) shows an example TEM image. We further estimate the TOP shell adds about 0.5 nm to the nanoparticles' radius, giving the particles an average hydrodynamic diameter of approximately 4 nm.

Synthesis of SBA-15 Mesoporous Materials

SBA-15 is a mesoporous silica sieve containing pores with a narrow pore size distribution that are arranged in a highly ordered, uniform hexagonal lattice.²⁹ SBA-15 matrices with two pore sizes were synthesized. Both syntheses used micelles of the nonionic triblock copolymer Pluronic P123 as the template. For the smaller pore diameter (6 nm), we followed the procedure reported by Zhao *et al.*³⁰ with modifications to the thermal treatments during synthesis based on the study by Brodie-Linder *et al.*³¹ Tetraethylorthosilicate (TEOS) was used as the silica source and HCl was used as the acid catalyst for the silica condensation reaction. The Pluronic (4.0 g) was dissolved in a solution of distilled water and 38% HCl (125 and 25 g, respectively). After stirring for 3 hr at 30 C, the TEOS (8.6 g) was added, and the solution was vigorously stirred for an additional 10 minutes. Then, the flask was sealed and the solution was kept for 24 hr at the same temperature. At this point, the temperature was adjusted to 100 C, and the mixture was again kept for 24 hr under reflux in static conditions. The resulting white solid was passed through a Buchner filter while being washed with 300 ml of water to eliminate the acid and excess reactants. It was then dried at room temperature for 24 hr, and then placed in a furnace where it was heated in air at 550 C for 18 hr. A white powder of SBA-15 was then collected. SBA-15 powders synthesized in this way have a typical grain size of 1 μm^3 with the grains containing straight and highly parallel, monodisperse pores in a hexagonal packing.^{32,33} Example TEM images of the SBA-15 are shown in Figs. S2(A) and S2(B) of the SI. The porosity of the SBA-15 was approximately 1

cm^3g^{-1} , as determined by adsorption isotherms. (The porosity is the total pore volume and can be deduced from the amount of adsorbate at a relative pressure of 0.95 in adsorption isotherms.) The pore diameter of the SBA-15, $D_p \approx 6$ nm, was obtained using the Barrett-Joyner-Halenda (BJH) method.³⁴ In addition, the pore diameter and lattice constant of the hexagonal pore lattice were estimated from the TEM images to be 5.0 ± 0.6 nm and 9.7 ± 0.4 nm, respectively.

To obtain SBA-15 with larger pore size, we followed the synthesis reported by Kruk *et al.*,³⁵ in which hexane was used to expand the Pluronic micelles. The synthesis proceeded by dissolving 0.027 g NH_4F and 2.4 g P123 in 84 mL 1.3 M HCl solution at room temperature. The mixture was then moved to a water bath at 15 C and kept there for 1 hr, after which a mixture of 5.17 g TEOS and 8.45 g hexane was added. The reaction mixture was kept at 15 C under continuous stirring for an additional 24 hr. The mixture was then transferred into a teflon-lined autoclave and heated to 130 C for 24 hr. The resulting powder was washed twice with ethanol and water, dried in a vacuum oven, and then calcined at 550 C under air to remove the surfactant. The white SBA-15 powder was then recovered and characterized. Example TEM images of the SBA-15 from this synthesis are shown in Figs. S2(C) and S2(D) of the SI. Using adsorption isotherms, the porosity was found to be approximately $1.12 \text{ cm}^3 \text{ g}^{-1}$. The pore diameter was determined by the improved Kruk-Jaroniec-Sayari method,³⁶ which is appropriate for larger-pore SBA-15 molecular sieves, and was found to be $D_p \approx 12$ nm. In addition, the pore diameter and lattice constant of the hexagonal pore lattice were estimated from the TEM images to be 10.5 ± 0.9 nm and 14.9 ± 0.3 nm, respectively.

XPCS

XPCS experiments were performed at the CHX beamline at the NSLS-II synchrotron facility at Brookhaven National Laboratory. Samples were contained in sealed stainless steel holders with 1.5 mm thickness and polyimide windows for transmission x-ray scattering measurements. The samples were prepared directly in the holders by combining appropriate

quantities of the SBA-15 matrix and glycerol/nanoparticle suspension to achieve 90% filling of the total available pore volume by the suspension. (Such filling has been found to cancel fully the Bragg peaks of the empty matrix in contrast-matching neutron scattering while leaving no observable fluid outside the pores.³⁷) As the glycerol strongly wets the SBA-15 surfaces, the suspension was taken up quickly by the matrix through capillary action. After the holders were filled, the samples were left overnight at 40 C to ensure complete filling of the channels and equilibration of the system.

The sample holders were positioned in a temperature-control stage on the beam line. A partially coherent x-ray beam of energy 9 keV and size $10 \times 10 \mu\text{m}^2$ was incident on the sample, and an area detector 10.1 m after the sample measured the scattering intensity over the wave-vector range $0.02 \text{ nm}^{-1} < q < 0.65 \text{ nm}^{-1}$. At each temperature typically two measurements were performed, one at 750 fps for 1000 frames and the other at 0.5 fps for 600 frames. The beam attenuated sufficiently to make any effects of x-ray exposure on the measured dynamics negligible, and the beam was also moved to a new position on the sample between each measurement to avoid any cumulative effects of the x-ray exposure. (See Sec. II of the SI for a diagnostic of x-ray exposure effects.) All measurements were conducted at least one hour after reaching each temperature to ensure its stabilization. The primary quantity obtained in the XPCS measurements was the time autocorrelation function of the scattered intensity,

$$g_2(q, t) = \frac{\langle I(\mathbf{q}, t')I(\mathbf{q}, t' + t) \rangle}{\langle I(\mathbf{q}, t') \rangle^2} \quad (1)$$

where $I(\mathbf{q}, t')$ is the intensity measured at wave vector \mathbf{q} and measurement time t' , and the averages are over t' and over detector pixels within a small range of wave-vector magnitude q . At large delay times t , $g_2(q, t)$ approaches unity if the system is ergodic. At $t \rightarrow 0$, it approaches $1 + \beta$, where β , known as the optical contrast, is the variance of the fluctuations in intensity divided by $\langle I \rangle^2$. The optical contrast depends on instrumental factors such as the coherence of the incident beam, the solid angle subtended by a detector pixel, and the sample thickness.³⁸ In the measurements on the 6-nm SBA-15, $\beta \approx 0.11$, while in the measurements

on the 12-nm SBA-15, $\beta \approx 0.15$ due to modifications to the x-ray optics between the two sets of measurements.

Results

Figure 1 shows the x-ray scattering intensity $I(q)$ from the SBA-15 matrix with 12-nm pores when filled with pure glycerol and when filled with the gold nanoparticle suspension. Both profiles show a pronounced peak at $q_p \approx 0.473 \text{ nm}^{-1}$, which we interpret as the first-order Bragg peak resulting from the hexagonally ordered pores in the SBA-15. (Note the lattice constant implied by this peak position, $4\pi/\sqrt{3}q_p \approx 15.3 \text{ nm}$, is consistent with the pore spacing determined from the TEM measurements, $14.9 \pm 0.3 \text{ nm}$.) To aid comparison of the shapes of the curves, each $I(q)$ is normalized with respect to the height of this peak. Above $q \approx 0.3 \text{ nm}^{-1}$, the shapes of the two profiles are very similar, indicating that the mesoporous silica dominates the scattering at high q . At lower q , the shapes differ, and matrix containing the nanoparticle suspension shows enhanced scattering intensity reflecting the contribution from the gold nanoparticles. Analysis of the XPCS results to characterize the nanoparticle dynamics was hence restricted to wave vectors below a maximum, $q_{max} \approx 0.25 \text{ nm}^{-1}$. The size of the contribution to $I(q)$ from the nanoparticles varied with location in the sample probed by the microbeam, suggesting spatial inhomogeneity in the concentration of nanoparticles. However, for all measurements, the matrix contributed substantially to the scattering intensity even at low q , influencing our interpretation of the XPCS results described below. Equivalent results for $I(q)$ from the 6-nm pore SBA-15 matrix are shown in Fig. S4 of the SI.

Figure 2(a) shows $g_2(q, t)$ at $q = 0.04 \text{ nm}^{-1}$ measured on the filled SBA-15 with 12-nm pores at temperatures ranging from 310 K to 380 K, and Fig. 2(b) shows correlation functions at $q = 0.10 \text{ nm}^{-1}$ for the filled SBA-15 with 6-nm pores between 403 K to 483 K. Figure 2(c) shows correlation functions at several wave vectors for the filled SBA-15 with 12-nm pores

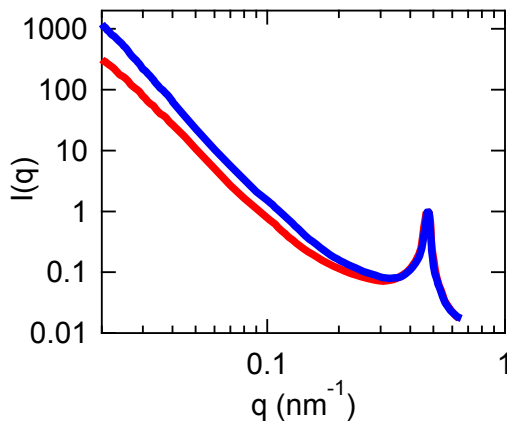


Figure 1: X-ray scattering intensity $I(q)$ measured on the SBA-15 matrix with 12-nm pores when filled with pure glycerol (red) and when filled with the gold nanoparticle suspension (blue). Both profiles show a pronounced peak at $q \approx 0.473 \text{ nm}^{-1}$ resulting from spatial correlations among the SBA-15 pores, which are arranged in a hexagonal lattice with lattice spacing $\approx 15.3 \text{ nm}$. To aid comparison, the curves have been normalized with respect to the height of this peak.

at 310 K. For both pore sizes, the correlation functions display a partial decay that moves to shorter delay times with increasing temperature. We associate this decay with motion of the gold nanoparticles within the pores. We further interpret the fact that the system is not ergodic (*i.e.*, $g_2(q, t)$ does not decay fully to one) as a consequence of the contribution to the scattering from the mesoporous silica, which shows a very slow structural relaxation. The dynamics of the nanoparticles in the 6-nm pores are significantly slower than in the 12-nm pores, as illustrated by the fact that the partial decays in $g_2(q, t)$ in Fig. 2(b) occur at larger t than in Fig. 2(a) despite the higher measurement temperatures. In both cases, these dynamics are far slower than expected based on the diffusivity of the gold nanoparticles in bulk glycerol. This difference is illustrated by the result for $g_2(q, t)$ at $q = 0.04 \text{ nm}^{-1}$ measured on the bulk glycerol/nanoparticle suspension at 263 K, which is shown by the open squares in Fig. 2(a). The dashed line through the bulk data shows the result of a fit using an exponential decay,

$$g_2(q, t) = 1 + b \exp(-t/\tau) \quad (2)$$

from which the diffusion coefficient D can be extracted through the relation $\tau = 1/Dq^2 = \frac{6\pi\eta R}{k_B T q^2}$, where η is the viscosity of glycerol. Despite the viscosity of glycerol decreasing approximately 2 to 3 orders of magnitude between 263 K and the temperature range of the measurements in the 12-nm pores (310 K to 380 K),^{39,40} the decay times are similar.

Analysis

As described above, both the gold nanoparticles and SBA-15 matrix contribute appreciably to the scattering below $q_{max} \approx 0.25 \text{ nm}^{-1}$. In this wave-vector range the XPCS measurements hence detected a heterodyne signal, wherein the scattering from the matrix and from the nanoparticles mixed coherently.⁴¹ For such heterodyne scattering, the intensity autocorrelation function $g_2(q, t)$ can be expressed as

$$g_2(q, t) = 1 + \beta \left(X^2 |g_{1,\text{Au}}(q, t)|^2 + 2X(1-X) \text{Re} [g_{1,\text{Au}}(q, t) g_{1,\text{SBA}}^*(q, t)] + (1-X)^2 |g_{1,\text{SBA}}(q, t)|^2 \right) \quad (3)$$

where $g_{1,\text{Au}}(q, t)$ and $g_{1,\text{SBA}}(q, t)$ are the intermediate scattering functions of the nanoparticles and the SBA-15 matrix, respectively, and X is the mixing ratio that is a measure of the fractional contribution to the scattering intensity from the nanoparticles.

Since the scattering from the nanoparticles contributed appreciably to the total scattering only below $q_{max} \approx 0.25 \text{ nm}^{-1}$, the measurements probed the nanoparticle motion over a range of length scales above a lower limit of approximately $q_{max}^{-1} \approx 4 \text{ nm}$. Further, since the particles had a hydrodynamic diameter of about 4 nm, their motion within the 12-nm pores in the directions transverse to the pore axes was restricted to displacements less than about 8 nm, and within the 6-nm pores the transverse displacements were restricted to roughly 2 nm. Therefore, the measurements accessed primarily the nanoparticle motion along the direction of the pore axes. To interpret $g_{1,\text{Au}}(q, t)$ under this condition, we consider a pore that is oriented along a direction $\hat{\mathbf{x}}$ at an angle θ to the scattering wave vector direction $\hat{\mathbf{q}}$, as depicted in the schematics in Fig. 3. We model particle motion down the pore as

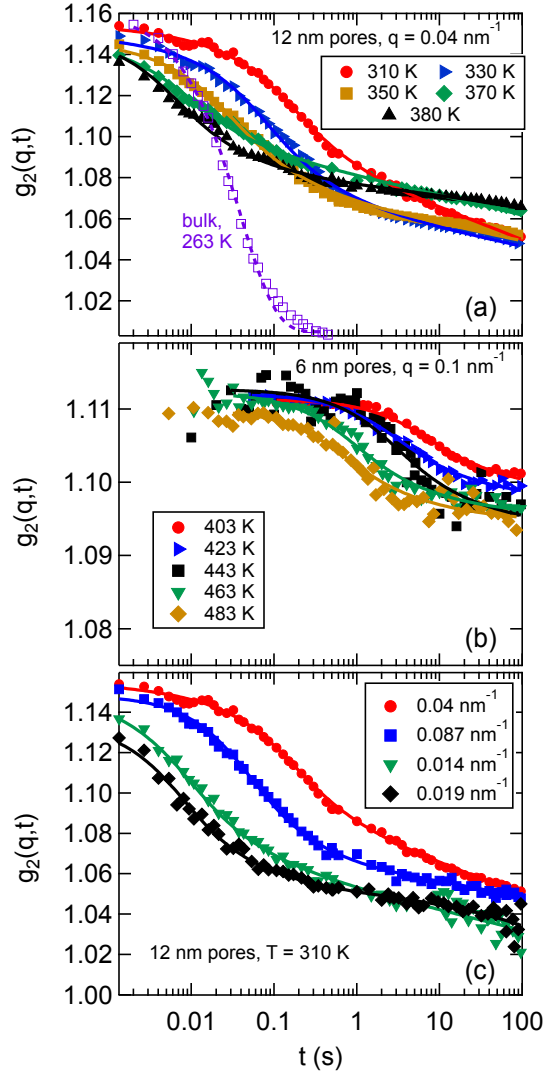


Figure 2: XPCS intensity autocorrelation function $g_2(q, t)$ measured on SBA-15 matrices filled with gold nanoparticle suspensions with (a) 12-nm pores at $q = 0.04 \text{ nm}^{-1}$ and at several temperatures, (b) 6-nm pores at $q = 0.10 \text{ nm}^{-1}$ and at several temperatures, and (c) 12-nm pores at 310 K and at several wave vectors, as indicated in the legends. The solid lines show the results of fits using a model of heterodyne scattering, Eq. (3), as described in the text. The open squares in (a) show $g_2(q, t)$ measured on the bulk gold suspension at 263 K at $q = 0.04 \text{ nm}^{-1}$, and the dashed line shows the result of a fit using an exponential decay, Eq. (2).

simple diffusion in one dimension wherein the particles have a probability distribution of displacements Δx parallel to the pore axis in a time duration t that is Gaussian, $p(\Delta x, t) = \exp(-\Delta x^2/4Dt)/\sqrt{4\pi Dt}$, and a mean squared displacement given by $\langle \Delta x^2(t) \rangle = 2Dt$, where

D is the diffusion coefficient. To understand how these dynamics dictate $g_{1,\text{Au}}(q, t)$, we assume the nanoparticles are sufficiently dilute that their dynamics are independent, so that the intermediate scattering function contains only self terms,

$$g_{1,\text{Au}}(\mathbf{q}, t) = \left\langle \frac{1}{N} \sum_{j=1}^N \exp [i\mathbf{q} \cdot (\mathbf{r}_j(t+t') - \mathbf{r}_j(t'))] \right\rangle_{t'} \quad (4)$$

where $\mathbf{r}_j(t')$ is the position of particle j at time t' , and N is the number of particles within the scattering volume. That is, $g_{1,\text{Au}}(\mathbf{q}, t)$ depends on the particle displacements projected onto $\hat{\mathbf{q}}$. For diffusion along the pore axis, that projected motion is similarly simple diffusion except with an effective diffusion coefficient $D_{eff} = D \cos^2 \theta$. For such diffusion, the intermediate scattering function decays as a simple exponential,

$$g_{1,\text{Au}}(\mathbf{q}, t; \theta) = \exp(-q^2 D_{eff} t) = \exp(-q^2 D t \cos^2 \theta) \quad (5)$$

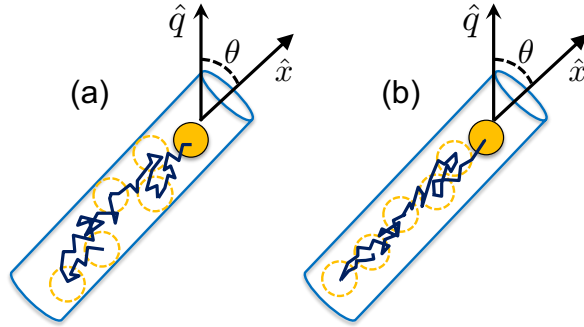


Figure 3: Schematics depicting different scenarios for a nanoparticle diffusing in glycerol within an SBA-15 pore. In (a) the particle's trajectory is punctuated by repeated adsorption to the pore walls. In (b), the particle is restricted to the central region of the pore because of an immobile layer of glycerol adjacent to the walls.

Since the SBA-15 samples are powders, they contain grains with a uniform distribution of orientations. Therefore, at any given scattering wave vector \mathbf{q} , the intermediate scattering

function will correspond to an average over pore orientations,

$$g_{1,\text{Au}}(q, t) = \langle g_{1,\text{Au}}(\mathbf{q}, t; \theta) \rangle_{\theta} = \frac{1}{2} \int_{-1}^1 \exp(-q^2 D t \cos^2 \theta) d(\cos \theta). \quad (6)$$

Evaluating this average leads to

$$g_{1,\text{Au}}(q, t) = \frac{\sqrt{\pi}}{2} \frac{\text{erf}(\sqrt{\Gamma t})}{\sqrt{\Gamma t}} \quad (7)$$

where $\Gamma = q^2 D$, and $\text{erf}()$ is the error function.

Regarding the intermediate scattering function of the SBA-15, the XPCS measurements capture slow structural dynamics, as evidenced from the fact that the $g_2(q, t)$ curves in Fig. 2 do not plateau to a constant value at large t but show a slight decay. (For reference, Fig. S5 in the SI shows a plot of $g_2(q, t)$ measured on the 12-nm pore SBA-15 filled with pure glycerol in the absence of nanoparticles.) We identify these slow dynamics with slow stress relaxation similar to that observed with XPCS in other mesoporous solids.^{38,42} Specifically, we believe the grains in the packed powder of SBA-15 slowly re-position to relieve internal stress in the jammed packing. Models of such internal stress relaxation, which consider the strain-like motion in response to stress dipoles,⁴³ predict a compressed-exponential correlation function,

$$g_{1,\text{SBA}}(q, t) = \exp[-(t/\tau_S)^{1.5}], \quad (8)$$

which has been shown to describe accurately the correlation function in these other cases.^{38,42} We thus fit the results for $g_2(q, t)$ using Eq. (3) with $g_{1,\text{Au}}(q, t)$ and $g_{1,\text{SBA}}(q, t)$ given by Eq. (7) and Eq. (8), respectively. The solid lines in Fig. 2 display results of such fits. The parameters included in the fits were X , Γ , and τ_S . Typically, the fits found $\tau_S > 1000$ s with significant uncertainty, reflecting the slow decay of $g_2(q, t)$ that is only partially captured in the data. However, the precise values of τ_S , and indeed the precise lineshape used to fit the slow decay in $g_2(q, t)$ are inconsequential to the results characterizing the nanoparticle dynamics, which

is our main focus. The values of X obtained from the fits, which tend to decrease with increasing q , varied from approximately 0.3 to 0.6 for the 12-nm pores and 0.1 to 0.3 for the 6-nm pores, consistent with the range expected based on the ratio of $I(q)$ for the silica matrices filled with nanoparticle suspension and with pure glycerol.

As the agreement between the fits and data in Fig. 2 demonstrates, the initial decay of $g_2(q, t)$ is accurately captured by the model of one-dimensional diffusion of the nanoparticles within the pores described above. Figures 4(a) and (b) show the decay rates Γ obtained from the fits as a function of q^2 at several temperatures for the 12-nm pores and 6-nm pores, respectively. At all temperatures, Γ varies linearly with q^2 as expected for diffusive dynamics. The solid lines in Figs. 4(a) and (b) show the results of fits using the form $\Gamma = q^2 D$, from which the temperature-dependent diffusion coefficients D of the nanoparticles are obtained.

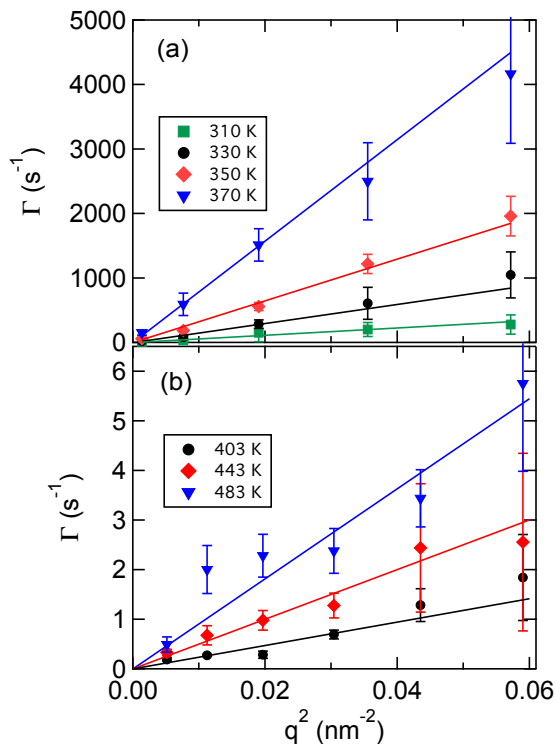


Figure 4: Decay rate Γ obtained from fits using Eq. (7) as a function of wave-vector squared at various temperatures indicated in the legend for (a) 12-nm pores and (b) 6-nm pores. The lines display the results of linear fits from which the nanoparticle diffusion coefficient is obtained.

Figure 5 shows the nanoparticle diffusion coefficients as a function of inverse temperature. As noted above, the mobility of the nanoparticles confined to the pores is highly suppressed with respect to that in bulk glycerol. However, the temperature dependence of the diffusivity appears to track, at least approximately, that of the inverse of the viscosity of glycerol. Specifically, the red dashed line in Fig. 5 through the diffusion coefficients in the 12-nm pores shows the diffusion coefficient expected for the nanoparticles based on the Stokes-Einstein relation, $D = \frac{k_B T}{6\pi\eta R}$, if they were in a fluid with viscosity η equal to 132 times that of glycerol's temperature-dependent viscosity.^{39,40} The line tracks the measured diffusion coefficients of the nanoparticles. Similarly, the blue dashed line, which tracks D of the particles in the 6-nm pores, shows the diffusion coefficients expected for the nanoparticles in a fluid with a viscosity equal to 820,000 times that of glycerol. From these comparisons we hence conclude that the gold nanoparticles in glycerol confined to mesoporous SBA-15 undergo diffusion that is extremely slowed compared with that in bulk glycerol but that nevertheless varies with temperature approximately as expected based on the viscosity of glycerol.

Discussion

Several possible mechanisms might contribute to the very small diffusion coefficients of the gold nanoparticles within the SBA-15 and their temperature dependence. One contribution is the enhancement to the hydrodynamic drag on the nanoparticles due of the confinement. The corrections to Stokes drag on a sphere translating in a cylindrical channel have been the subject of detailed fluid-dynamics calculations and experiments.^{44,45} Based on these studies, we estimate the Stokes drag on a 4-nm sphere is enhanced over that in bulk by a factor of roughly 20 in a 6-nm pore and by a factor of roughly 3 in a 12-nm pore, depending of the position of the sphere relative to the central axis of the pore. While not insignificant, these increases are too small to account fully for the large suppression in diffusivity observed in the experiments.

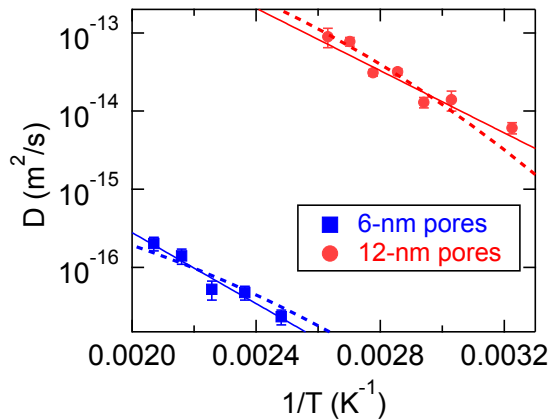


Figure 5: Diffusion coefficients D of the gold nanoparticles in the 12-nm (red circles) and 6-nm (blue squares) pores as a function of inverse temperature. The solid lines display the results of fits using an Arrhenius form for D , Eq. (9). The dashed lines are the diffusion coefficients for gold nanoparticles with hydrodynamic diameter of 4 nm in a fluid with a viscosity proportional to the temperature-dependent viscosity of glycerol. Specifically, the red dashed line is the diffusion coefficient of particles in a fluid with a temperature-dependent viscosity equal to 132 times that of glycerol, and the blue dashed line is the diffusion coefficient in a fluid with a viscosity 820,000 times that of glycerol.

A second possible contribution involves surface interactions that lead to adsorption and desorption of the particles at the internal silica surfaces of the pores. Reduced mobility dictated by adsorption and desorption has been observed for nanoparticles in planer confinement^{13,15,17} and for fluorescent probe molecules in nanoporous membranes.⁴⁶ We hypothesize that the nanoparticles within the pores might follow trajectories like that depicted schematically in Fig. 3(a), in which the nanoparticles repeatedly adsorb to the pore walls, where they remain for an average residence time τ_r . Upon desorption, the particles diffuse such that they travel along the pore axis \hat{x} a typical distance L before re-adsorbing. Such desorption-mediated motion would lead continuous time random walks (CTRWs) that obey Fickian diffusion at large lengths. To estimate L , we assume the particles traverse along the pore axis a distance approximately equal to their lateral confinement, so $L \approx 8$ nm in the 12-nm pores and $L \approx 2$ nm in the 6-nm pores. The diffusion coefficient would hence be $D = L^2/\tau_r$. Since the desorption should be thermally activated, the diffusion coefficient can be expected

to follow an Arrhenius form,

$$D = L^2 f_0 \exp(-E_A/k_B T), \quad (9)$$

where E_A is the activation energy, and f_0 is an attempt frequency. The red and blue solid lines in Fig. 5 show the results of fits to D using Eq. (9) for the 12-nm and 6-nm pores, respectively. The fits for the two pores sizes, which describe the temperature dependence accurately, find very similar activation energies, $(4600 \pm 300)k_B$ for the 12-nm pores and $(5200 \pm 600)k_B$ for the 6-nm pores. The large difference in diffusion coefficients between the pore sizes is instead captured by f_0 , which is $(2.0 \pm 0.1) \times 10^8 \text{ s}^{-1}$ for the 12-nm pores but only $(2.5 \pm 0.3) \times 10^6 \text{ s}^{-1}$ for the 6-nm pores. Such a large difference in attempt frequencies is difficult to interpret. Naively, one would expect that the difference in D between the pore sizes would be due to differing activation energies, particularly since the smaller radius of curvature in the 6-nm pores should lead to larger effective contact area between the particles and pore walls, raising questions about whether adsorption and desorption indeed play a major role in dictating nanoparticle mobility in the pores. On the other hand, the small radius of curvature of the 6-nm pores could also lead to more frequent adsorption than we assume, making L much smaller than estimated, which in turn would imply a larger f_0 . Therefore, we cannot conclusively rule out that the nanoparticle diffusion is set by adsorption and desorption events.

A third, intriguing possible contribution to the suppressed nanoparticle diffusivity in the SBA-15 is slowed structural dynamics in the glycerol induced by the nanoconfinement. Nanoconfinement is known to alter the structural dynamics and hence viscosity of liquids and to change the glass transition temperature T_g of glass-forming liquids like glycerol.^{47,48} In the case of glycerol, experiments have reported that nanoconfinement can both increase or decrease T_g , which is approximately 190 K in bulk.^{49–52} This variation in response of the structural dynamics to confinement is attributed to the different influences of the finite size

effects versus the surface interactions between the liquid molecules and confining matrix, which depend on the specific surface chemistry of the matrix.⁵³ Surface interactions can be expected to be particularly strong between SBA-15 and glycerol since surface hydroxyl groups (silanols) on the amorphous silica can form hydrogen bonds with the glycerol. To account for surface interactions, researchers have proposed models in which a confined fluid contains two regions, a relatively immobile, near-surface layer close to the confining walls and a more mobile, internal volume. Indeed, Trofymuk *et al.* employed FTIR spectroscopy to investigate the structural dynamics of glycerol in SBA-15 and identified an interfacial layer with an estimated thickness of 0.7 nm, which is similar to the size of a glycerol molecule.⁵⁰ Levchenko *et al.* further used ¹³C NMR to measure the reorientational dynamics of glycerol in the mesoporous silica matrix MCM-41 with 2.2 nm pores and found the dynamics were slowed by more than 3 orders of magnitude at room temperature due to the confinement.⁵⁴ We note these previous studies investigated neat glycerol under nanoconfinement. The addition of nanoparticles within the pores makes the possible consequences of finite size effects and surface interactions more complicated and potentially more dramatic since both the pore walls and particles provide confining surfaces. For instance, in the 6-nm pores the 4-nm nanoparticles are never more than 1 nm from a pore wall. Thus, strong slowing of the glycerol structural dynamics like that reported by Levchenko *et al.* could potentially be a major contributor to the large reduction in nanoparticle diffusion that we observe.

The presence of a relatively immobile surface layer could further position the nanoparticles preferentially near the center of the pores, leading to diffusive trajectories like that depicted in Fig. 3(b). Such restriction to the pore centers would help explain the success of Eq. (7) in modeling $g_{1,\text{Au}}(q, t)$ to wave vectors as large as $q_{max} = 0.25 \text{ nm}^{-1}$. Specifically, since the nanoparticle motion is expected to transition from 3D-like to 1D-like at a length scale set by the lateral confinement, $g_{1,\text{Au}}(q, t)$ can be expected to change from Eq. (7) in the limit of low q to something closer to a simple exponential decay at high q . Based on an estimate of 8 nm for the extent of lateral motion of the nanoparticles in the 12-nm pores,

one might expect to see evidence of this crossover in the lineshape below q_{max} ; however, restriction to the pore center due to an interfacial layer would push the crossover to higher q .

Conclusion

In conclusion, we have observed that gold nanoparticles in glycerol confined to nanometer-scale pores undergo diffusion that is dramatically slower than that of the nanoparticles in bulk glycerol. We consider several mechanisms that might contribute to this reduction in diffusivity including transient adsorption of the nanoparticles to the pore walls and suppression of the structural dynamics of the glycerol solvent. We conclude suppression of the structural dynamics of the glycerol due to the confinement imposed by the pore surfaces in conjunction with the presence of the nanoparticles is likely a major contributor. We note that the desorption-mediated CTRW dynamics would have non-Gaussian statistics that contrast with the Brownian motion in viscous glycerol, and in principle analysis of the higher-order time correlations in the x-ray speckle patterns could possibly distinguish between the two.³⁸ While the current measurements do not have adequate statistics for such analysis, future XPCS experiments with improved statistics potentially could. In addition, studies of these same nanoparticles in glycerol in planar confinement with liquid-cell TEM could illuminate possible effects of surface interactions and potentially shed light on the role of surface adsorption versus solvent restructuring in reducing the nanoparticle mobility. Furthermore, additional XPCS studies, such as those employing SBA-15 with silanized surfaces that suppress hydrogen bonding with the glycerol or employing a non-polar liquid instead of glycerol as the solvent, would make for interesting comparisons with these results. More broadly these experiments have shown how XPCS can be an effective method to probe nanoparticle dynamics under nanoconfinement in matrices where alternative techniques are unfeasible. Future XPCS studies that explore this capability further would be valuable.

Acknowledgement

We thank Yihao Chen for helpful discussions. Funding was provided by the NSF (CBET-1804721 and DMR-1610875). This work used resources of the National Synchrotron Light Source II (Beamline 11-ID), which is a U.S. DOE Office of Science Facilities, at Brookhaven National Laboratory under Contract No. DE-SC0012704.

References

- (1) Molnar, I. L.; Johnson, W. P.; Gerhard, J. I.; Willson, C. S.; O’Carroll, D. M. Predicting colloid transport through saturated porous media: A critical review. *Water Resour. Res.* **2015**, *51*, 6804–6845.
- (2) Vasilyev, O. A.; Dietrich, S.; Kondrat, S. Nonadditive interactions and phase transitions in strongly confined colloidal systems. *Soft Matter* **2018**, *14*, 586–596.
- (3) Babayekhorasani, F.; Dunstan, D. E.; Krishnamoorti, R.; Conrad, J. C. Nanoparticle diffusion in crowded and confined media. *Soft Matter* **2016**, *12*, 8407–8416.
- (4) Burada, P. S.; Hänggi, P.; Marchesoni, F.; Schmid, G.; Talkner, P. Diffusion in Confined Geometries. *ChemPhysChem* **2009**, *10*, 45–54.
- (5) Faez, S.; Lahini, Y.; Weidlich, S.; Garmann, R. F.; Wondraczek, K.; Zeisberger, M.; Schmidt, M. A.; Orrit, M.; Manoharan, V. N. Fast, Label-Free Tracking of Single Viruses and Weakly Scattering Nanoparticles in a Nanofluidic Optical Fiber. *ACS Nano* **2015**, *9*, 12349–12357.
- (6) Raccis, R.; Nikoubashman, A.; Retsch, M.; Jonas, U.; Koynov, K.; Butt, H.-J.; Likos, C. N.; Fytas, G. Confined Diffusion in Periodic Porous Nanostructures. *ACS Nano* **2011**, *5*, 4607–4616.

- (7) Jacob, J. D. C.; He, K.; Retterer, S. T.; Krishnamoorti, R.; Conrad, J. C. Diffusive dynamics of nanoparticles in ultra-confined media. *Soft Matter* **2015**, *11*, 7515–7524.
- (8) Fringes, S.; Holzner, F.; Knoll, A. W. The nanofluidic confinement apparatus: studying confinement-dependent nanoparticle behavior and diffusion. *Beilstein J. Nanotechnol.* **2018**, *9*, 301–310.
- (9) Giraudet, C.; Knoll, M. S. G.; Galvan, Y.; Sü"s, S.; Segets, D.; Vogel, N.; Rausch, M. H.; Fröba, A. P. Diffusion of Gold Nanoparticles in Inverse Opals Probed by Heterodyne Dynamic Light Scattering. *Transp. Porous Media* **2020**, *131*, 723–737.
- (10) Wu, H.; Schwartz, D. K. Nanoparticle Tracking to Probe Transport in Porous Media. *Acc. Chem. Res.* **2020**, *53*, 2130–2139.
- (11) Woehl, T. J.; Prozorov, T. The Mechanisms for Nanoparticle Surface Diffusion and Chain Self-Assembly Determined from Real-Time Nanoscale Kinetics in Liquid. *J. Phys. Chem. C* **2015**, *119*, 21261–21269.
- (12) Verch, A.; Pfaff, M.; de Jonge, N. Exceptionally Slow Movement of Gold Nanoparticles at a Solid/Liquid Interface Investigated by Scanning Transmission Electron Microscopy. *Langmuir* **2015**, *31*, 6956–6964.
- (13) Chee, S. W.; Baraissov, Z.; Loh, N. D.; Matsudaira, P. T.; Mirsaidov, U. Desorption-Mediated Motion of Nanoparticles at the Liquid–Solid Interface. *J. Phys. Chem. C* **1985**, *120*, 20462–20470.
- (14) Powers, A. S.; Liao, H.-G.; Raja, S. N.; Bronstein, N. D.; Alivisatos, A. P.; Zheng, H. Tracking Nanoparticle Diffusion and Interaction during Self-Assembly in a Liquid Cell. *Nano Lett.* **2017**, *17*, 15–20.
- (15) Tian, X.; Zheng, H.; Mirsaidov, U. Aggregation dynamics of nanoparticles at solid-liquid interfaces. *Nanoscale* **2017**, *9*, 10044–10050.

- (16) Yesibolati, M. N.; Mortensen, K. I.; Sun, H.; Brostrøm, A.; Tidemand-Lichtenberg, S.; Mølhave, K. Unhindered Brownian Motion of Individual Nanoparticles in Liquid-Phase Scanning Transmission Electron Microscopy. *Nano Lett.* **2020**, *20*, 7108–7115.
- (17) Jamali, V.; Hargus, C.; Ben-Moshe, A.; Aghazadeh, A.; Ha, H. D.; Mandadapu, K. K.; Alivisatos, A. P. Anomalous nanoparticle surface diffusion in LCTEM is revealed by deep learning-assisted analysis. *Proc. Natl. Acad. Sci. U. S. A.* **2021**, *118*, e2017616118.
- (18) Leheny, R. L. XPCS: Nanoscale motion and rheology. *Curr. Opin. Colloid Interface Sci.* **2012**, *17*, 3–12.
- (19) Jiang, N.; Endoh, M. K.; Koga, T. ‘Marker’ grazing-incidence X-ray photon correlation spectroscopy: a new tool to peer into the interfaces of nanoconfined polymer thin films. *Polym. J.* **2013**, *45*, 26 – 33.
- (20) Cristofolini, L. Synchrotron X-ray techniques for the investigation of structures and dynamics in interfacial systems. *Curr. Opin. Colloid Interface Sci.* **2014**, *19*, 228 – 241.
- (21) Ruta, B.; Czakkel, O.; Chushkin, Y.; Pignon, F.; Nervo, R.; Zontone, F.; Rinaudo, M. Silica nanoparticles as tracers of the gelation dynamics of a natural biopolymer physical gel. *Soft Matter* **2014**, *10*, 4547–4554.
- (22) Koga, T.; Li, C.; Endoh, M. K.; Koo, J.; Rafailovich, M.; Narayanan, S.; Lee, D. R.; Lurio, L. B.; Sinha, S. K. Reduced Viscosity of the Free Surface in Entangled Polymer Melt Films. *Phys. Rev. Lett.* **2010**, *104*, 066101.
- (23) Koga, T.; Jiang, N.; Gin, P.; Endoh, M. K.; Narayanan, S.; Lurio, L. B.; Sinha, S. K. Impact of an Irreversibly Adsorbed Layer on Local Viscosity of Nanoconfined Polymer Melts. *Phys. Rev. Lett.* **2011**, *107*, 225901.

- (24) Johnson, K. J.; Glynos, E.; Maroulas, S.-D.; Narayanan, S.; Sakellariou, G.; Green, P. F. Confinement Effects on Host Chain Dynamics in Polymer Nanocomposite Thin Films. *Macromolecules* **2017**, *50*, 7241–7248.
- (25) Grein-Iankovski, A.; Riegel-Vidotti, I. C.; Simas-Tosin, F. F.; Narayanan, S.; Leheny, R. L.; Sandy, A. R. Exploring the relationship between nanoscale dynamics and macroscopic rheology in natural polymer gums. *Soft Matter* **2016**, *12*, 9321–9329.
- (26) Lee, J.; Grein-Iankovski, A.; Narayanan, S.; Leheny, R. L. Nanorod Mobility within Entangled Wormlike Micelle Solutions. *Macromolecules* **2017**, *50*, 406–415.
- (27) Guo, H.; Bourret, G.; Lennox, R. B.; Sutton, M.; Harden, J. L.; Leheny, R. L. Entanglement-Controlled Subdiffusion of Nanoparticles within Concentrated Polymer Solutions. *Phys. Rev. Lett.* **2012**, *109*, 055901.
- (28) Nygård, K.; Buitenhuis, J.; Kagias, M.; Jefimovs, K.; Zontone, F.; Chushkin, Y. Anisotropic de Gennes Narrowing in Confined Fluids. *Phys. Rev. Lett.* **2016**, *116*, 167801.
- (29) Chaudhary, V.; Sharma, S. An overview of ordered mesoporous material SBA-15: synthesis, functionalization and application in oxidation reactions. *J. Porous Mater.* **2017**, *24*, 741–749.
- (30) Zhao, D.; Feng, J.; Huo, Q.; Melosh, N.; Fredrickson, G. H.; Chmelka, B. F.; Stucky, G. D. Triblock Copolymer Syntheses of Mesoporous Silica with Periodic 50 to 300 Angstrom Pores. *Science* **1998**, *279*, 548–552.
- (31) Brodie-Linder, N.; Dosseh, G.; Alba-Simonesco, C.; Audonnet, F.; Impéror-Clerc, M. SBA-15 synthesis: Are there lasting effects of temperature change within the first 10min of TEOS polymerization? *Mater. Chem. Phys.* **2008**, *108*, 73 – 81.

- (32) Zhao, D.; Sun, J.; Li, Q.; Stucky, G. D. Morphological Control of Highly Ordered Mesoporous Silica SBA-15. *Chem. Mater.* **2000**, *12*, 275–279.
- (33) Hartmann, M.; Kunz, S.; Govindasamy, C.; Murugesan, V. Shaping of mesoporous molecular sieves. *Stud. Surf. Sci. Catal.* **2007**, *165*, 181–184.
- (34) Bardestani, R.; Patience, G. S.; Kaliaguine, S. Experimental methods in chemical engineering: specific surface area and pore size distribution measurements—BET, BJH, and DFT. *Can. J. Chem. Eng.* **2019**, *97*, 2781–2791.
- (35) Kruk, M.; Cao, L. Pore size tailoring in large-pore SBA-15 silica synthesized in the presence of hexane. *Langmuir* **2007**, *23*, 7247–7254.
- (36) Jaroniec, M.; Solovyov, L. A. Improvement of the Kruk- Jaroniec- Sayari method for pore size analysis of ordered silicas with cylindrical mesopores. *Langmuir* **2006**, *22*, 6757–6760.
- (37) Mhanna, R.; Hamid, A.; Dutta, S.; Lefort, R.; Noirez, L.; Frick, B.; Morineau, D. More room for microphase separation: An extended study on binary liquids confined in SBA-15 cylindrical pores. *J. Chem. Phys.* **2017**, *146*, 024501.
- (38) Madsen, A.; Leheny, R. L.; Guo, H.; Sprung, M.; Czakkel, O. Beyond simple exponential correlation functions and equilibrium dynamics in x-ray photon correlation spectroscopy. *New J. Phys.* **2010**, *12*, 055001.
- (39) Slie, W. M.; Madigosky, W. M. Pressure Dependence of the Elastic Moduli of Liquid Glycerol. *J. Chem. Phys.* **1968**, *48*, 2810–2817.
- (40) Ferreira, A. G.; Egas, A. P.; Fonseca, I. M.; Costa, A. C.; Abreu, D. C.; Lobo, L. Q. The viscosity of glycerol. *J. Chem. Thermodyn.* **2017**, *113*, 162 – 182.

- (41) Livet, F.; Bley, F.; Ehrburger-Dolle, F.; Morfin, I.; Geissler, E.; Sutton, M. X-ray intensity fluctuation spectroscopy by heterodyne detection. *J. Synchrotron Radiat.* **2006**, *13*, 453–458.
- (42) Hernández, R.; Nogales, A.; Sprung, M.; Mijangos, C.; Ezquerro, T. A. Slow dynamics of nanocomposite polymer aerogels as revealed by X-ray photocorrelation spectroscopy (XPCS). *J. Chem. Phys.* **2014**, *140*, 024909.
- (43) Bouchaud, J.-P.; Pitard, E. Anomalous dynamical light scattering in soft glassy gels. *Eur. Phys. J. E* **2001**, *6*, 231–236.
- (44) Ambari, A.; Gauthier-Manuel, B.; Guyon, E. Direct measurement of tube wall effect on the Stokes force. *Phys. Fluids* **1985**, *28*, 1559–1561.
- (45) Happel, J.; Brenner, H. *Low Reynolds number hydrodynamics*; Springer Netherlands, 1983.
- (46) Hohlbein, J.; Steinhart, M.; Schiene-Fischer, C.; Benda, A.; Hof, M.; Hübner, C. Confined Diffusion in Ordered Nanoporous Alumina Membranes. *Small* **2007**, *3*, 380–385.
- (47) Alcoutlabi, M.; McKenna, G. B. Effects of confinement on material behaviour at the nanometre size scale. *J. Phys.: Condens. Matter* **2005**, *17*, R461–R524.
- (48) Richert, R. Dynamics of Nanoconfined Supercooled Liquids. *Annu. Rev. Phys. Chem.* **2011**, *62*, 65–84.
- (49) Busselez, R.; Lefort, R.; Ji, Q.; Affouard, F.; Morineau, D. Molecular dynamics simulation of nanoconfined glycerol. *Phys. Chem. Chem. Phys.* **2009**, *11*, 11127–11133.
- (50) Trofymuk, O.; Levchenko, A. A.; Navrotsky, A. Interfacial effects on vitrification of confined glass-forming liquids. *J. Chem. Phys.* **2005**, *123*, 194509.
- (51) Zheng, W.; Simon, S. L. Confinement effects on the glass transition of hydrogen bonded liquids. *J. Chem. Phys.* **2007**, *127*, 194501.

- (52) Kilburn, D.; Sokol, P. E.; García Sakai, V.; Ashraf Alam, M. Confinement induces both higher free volume and lower molecular mobility in glycerol. *Appl. Phys. Lett.* **2008**, *92*, 033109.
- (53) Morineau, D.; Xia, Y.; Alba-Simionesco, C. Finite-size and surface effects on the glass transition of liquid toluene confined in cylindrical mesopores. *J. Chem. Phys.* **2002**, *117*, 8966–8972.
- (54) Levchenko, A. A.; Jain, P.; Trofymuk, O.; Yu, P.; Navrotsky, A.; Sen, S. Nature of Molecular Rotation in Supercooled Glycerol under Nanoconfinement. *J. Phys. Chem. B* **2010**, *114*, 3070–3074.

Graphical TOC Entry

